Modeling and Simulation of Activated Corrosion Products Behavior under Design-Based Variation of Neutron Flux Rate in AP-1000

F. Mahmood, H. Hu[a], L. Cao and G. Lu

School of Nuclear Science and Technology, Xi'an Jiaotong University, Xi'an, China
fiazmahmood@stu.xjtu.edu.cn

Abstract: The research on Activated Corrosion Products (ACPs) is gaining more significance motivated by the growing trend of innovative reactor designs in world energy market. In this research, application of a locally developed code CPA-AP1000 is extended to study progression of ACPs in primary circuit of AP-1000 under full power neutron flux and design based variation in the flux rate. The programing is executed in MATLAB while MCNP code is used to compute the neutron flux distribution in reactor core, under particular operating conditions. The mathematical model in the program is handled to account for calculation of ACPs for full power flux and varying flux rate scenarios. The simulations are carried out for steady state operation up to Middle of Cycle (MOC) and afterwards slow changes in neutron flux rate, derived by the Mechanical Shim (MSHIM) based power maneuvers, are introduced in the system. The results for major ACPs demonstrate that during period of normal full power operation short-lived ACPs build up promptly, rendering an immediate radiation source for inspection and maintenance crews. When neutron flux rate is slowly reduced and ultimately settled to a lower value, the saturation specific activity of corresponding radioisotopes changes accordingly. The short-lived ACPs rapidly attain a new lower saturation value of specific activity but those having long half-lives sluggishly decay and ultimately produce radiation sources, which hold for a longer period of time. The studies are further extended to compare the build-up and decay pattern of ^{56}Mn in primary coolant, core scale and piping structure. The specific activity due to ^{56}Mn in all parts (coolant, core and piping) of primary circuit builds up promptly under normal full power operation and rapidly declines following the reduction in neutron flux rate. The simulation results reveal that specific activity due to *ACPs* in core scale is the largest source under all operating conditions.

Key Words: Activated Corrosion Products, specific activity, CPA-AP1000, power maneuvering, neutron flux rate variation

1 Introduction

The ACPs impose a major radiological burden during routine surveillance, equipment handling and maintenance activities of RCS. The estimation of radiation dose caused by the ACPs in RCS of nuclear power plant (NPP) is effective for job planning and assessment of ORE to the surveillance

[a] Corresponding author
Tel: +86-29-82668648, Fax: +86-29-82667802
Email address: huasi_hu@mail.xjtu.edu.cn

and maintenance workers. The optimization of ORE caused by ACPs is mostly executed through the planning of routine maintenance during reactor shutdown periods. However, daily surveillance and emergency maintenance put forwards need of an urgent approach to RCS. Therefore, evaluation of activity caused by ACPs during various plant operating conditions is of utmost importance. When primary coolant containing ACPs passes through the flow channels of the primary coolant circuit it deposits the dissolved and suspended radionuclides on the cooling system inner surfaces [1]. The types of radionuclides formed, the levels of equilibrium activity reached and the rate at which the equilibrium is reached all are functions of various operating parameters of the reactor. These also include the composition of the materials in contact with the coolant, amount and the types of the impurities present in the coolant, operating power of the reactor, residence time of the coolant in the reactor core, temperatures and pressures, coolant flow rate, corrosion rate and filter efficiency. The major corrosion products and their reaction properties are described in Table 1 [2].

The radiological inventory of RCS mainly depends on the amount of ACPs present in primary coolant and deposited on the inner surfaces of the system walls, if fuel failure is ignored. The evaluation of radioactive crud sources in RCS of NPPs highly depends on plant operating conditions and design specifications. New operational strategies of modern reactor designs are coming up with effective contribution to meet variable demands in world energy. However, estimation of variation in activity level in RCS during application of design based operational strategies has turned out more challenging. In previous studies, typical PWRs are most widely focused in the subjected area of research. Recently, ACPs behavior in innovative reactor designs has also been studied [3-5] . The research efforts have been dedicated to understand the corrosion kinetics by developing CAT code [6]. Subsequently, another computer code CPA-AP1000 is locally developed to study the behavior of ACPs in the AP-1000 [7]. In this study, activity levels of the major corrosion products in RCS are evaluated during reactor full power operation and design based slow changes in neutron flux employing the CPA-AP1000.

Table 1. Corrosion products and their reaction properties

Sr.#	Reaction	Activated CP	Activation cross section	γ-ray energy
1	^{23}Na (n, γ) ^{24}Na (E_n >11.60 MeV)	^{24}Na ($T_{1/2}$=15.40 h)	0.53 b	4.10 MeV
2	^{58}Fe (n, γ) ^{59}Fe (E_n is thermal)	^{59}Fe ($T_{1/2}$=45.10 h)	0.90 b	1.17 MeV (99.99%) 1.33 MeV (99.99%)
3	^{98}Mo (n, γ) ^{99}Mo (E_n >3.10 MeV)	^{99}Mo ($T_{1/2}$=67.00 h)	0.45 b	0.78 MeV (8%) 0.74 MeV (8%)
4	^{59}Co (n, γ) ^{60}Co	^{60}Co ($T_{1/2}$=5.30 y)	20.00 b	1.17 MeV (99.99%) 1.33 MeV (99.99%)
5	^{55}Mn (n, γ) ^{56}Mn (E_n is thermal)	^{56}Mn ($T_{1/2}$=2.58 h)	13.40 b	2.13 MeV (15%) 1.81 MeV (24%) 0.85MeV (99%)

2 Mathematical model

The time-dependent model of activity in the primary coolant circuit is established by balancing the rate of production and loss of radioactive nuclei due to different exchange pathways. The pathways include activation of CPs due to power dependent value of flux, purification of coolant, deposition of the materials on surfaces, leakage from the system and radioactive decay of activated products. Different pathways leading to these production and loss mechanisms are schematically described in Fig. 1.

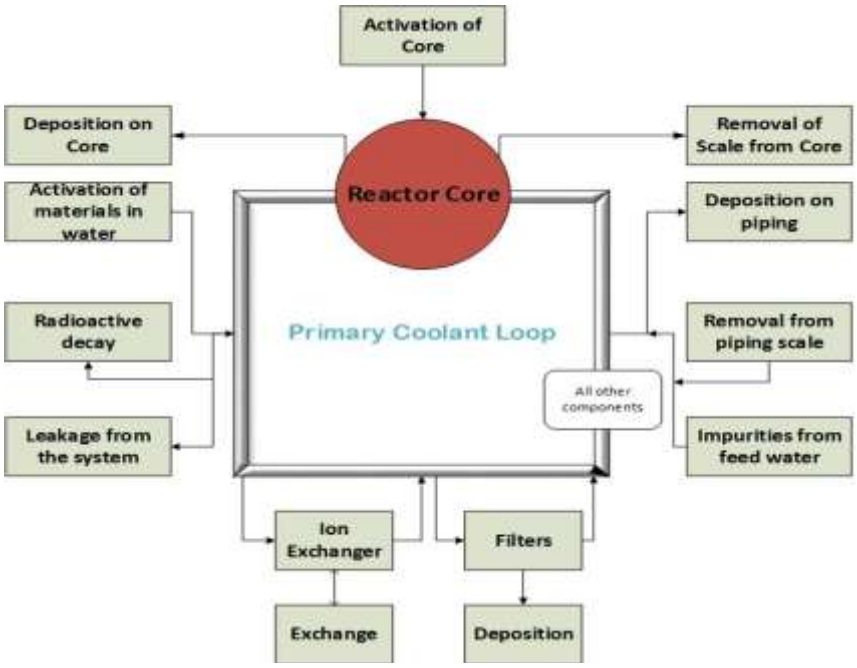

Fig. 1. Schematic of exchange pathways for modeling activation products in the primary coolant circuit

The mathematical model of the time-dependent behavior of dominant CPs in the primary coolant circuit of AP-1000 is based on the following assumptions.

- The composition of CPs corresponds to the chemical composition of originally corroding material.
- The material of walls of cooling system corrodes uniformly and homogeneously.
- The intrinsic activity is considered negligible.
- The deposition on surfaces in contact with cooling water is proportional to the concentration of CPs in water.
- The ion-exchangers and filters remove impurities in proportion to their concentration in the coolant.

The design-based variation in neutron flux rate is introduced into the system by Mechanical Shim (MSHIM) based power maneuvers. The neutron flux is treated as representative of reactor operating power. The change in neutron flux rate is modeled as directly affected by variation in reactor operating power. In order to incorporate the effect of power maneuverings, the power levels are modeled with the subsequent scheme. The time-dependent operating power $p(t)$ is defined in terms of normalized power parameter $f(t)$ and Rated Thermal Power (RTP) p_0 as following;

$$p(t) = f(t)p_0 \quad (1)$$

The parameter $f(t)$ is capable of describing reactor operation at various power levels and under *MSHIM* based power transients. The power parameter $f(t)$ describes any linear increase or decrease in reactor operational power as following;

$$f(t) = \begin{cases} p_1 & , t < t_s \\ p_1 - \mu(t - t_{ts}) & , t_{ts} \leq t < t_{te} \\ p_2 & , t \geq t_{te} \end{cases} \quad (2)$$

where p_1 and p_2 represent operating power in terms of percentage *RTP* before start and end of power maneuvering at time t_{ts} and t_{te} respectively, and μ is the slope of linear increase or decrease operating power.

The activation of CPs is affected by the time taken by a particle for traversing through the primary coolant circuit, and length of time it is exposed to the neutron flux. The effective neutron flux density ϕ_ϵ (n/cm^2.sec) links both of these time intervals as following;

$$\phi_\epsilon = \frac{1-e^{-\lambda T_c}}{1-e^{-\lambda T_L}}\phi_0 \quad (3)$$

where ϕ_0 is thermal neutron flux density (n/cm^2.sec) averaged over the geometry of core, λ is decay constant (sec^{-1}) of the activated nuclide of interest, T_c is time length for which a particle of coolant is exposed to the neutron flux and can be estimated as $H\rho A/w(t)$. The parameter H is core height, ρ is the density of the coolant at operating temperature and pressure, and $w(t)$ is time dependent mass flow rate. The circulating time of a particle through the primary coolant system is denoted by T_L for loop length L of the primary circuit and can be estimated as LT_c/H.

The concentration of target nuclides (atoms/cm^3) in the primary coolant, on piping and core surfaces have been denoted by N_w, N_p and N_c respectively. The concentrations of activated nuclides (atoms/cm^3) in the primary coolant water, on the inner walls of piping and core surfaces have been denoted by n_w, n_p, and n_c respectively. The rate of change of active material concentration in primary coolant is given by;

$$\frac{dn_w}{dt} = \sigma f(t)\phi_\epsilon N_w - \left(\sum_j \frac{\varepsilon_j Q_j}{V_w} + \sum_k \frac{l_k}{V_w} + \lambda\right) n_w + \frac{k_p}{V_w} n_p + \frac{k_c}{V_w} n_c \quad (4)$$

where σ is the group constant for the production of ithe sotope from target nuclide. The sum over j for $\varepsilon_j Q_j$ is given as following;

$$\varepsilon_j Q_j = \varepsilon_i Q_i + \varepsilon_f Q_f + \varepsilon_c Q_c + \varepsilon_p Q_p \quad (5)$$

where the quantities $\varepsilon_i Q_i$, $\varepsilon_f Q_f$, $\varepsilon_c Q_c$, $\varepsilon_p Q_p$ are removal rates (cm^3/sec) induced by ion exchanger, filter, core and pipe surfaces respectively. The term l_k is rate (cm^3/sec) at which the primary coolant is lost during kth leak, k_p and $kthe_c$ are rates (cm^3/sec) at which isotopes are removed from the scale on piping and core respectively. The first term in equation (4) represents the production of radioactive isotopes. The second term is rate at which active the nuclides are lost because of purification by the ion-exchanger and filter, deposition on the piping and core and decay of the activated nuclei. The third and fourth terms are the rates at which activity is re-introduced into the water because of erosion or dissolution of activity deposited on inner surfaces of piping and reactor core. The rate of change in target nuclide concentration in coolant water can be written as;

$$\frac{dN_w}{dt} = -\left(\sum_j \frac{\varepsilon_j Q_j}{V_w} + \sum_k \frac{l_k}{V_w} + \sigma f(t)\phi_\epsilon\right) N_w + \frac{k_p}{V_w} N_p + \frac{k_c}{V_w} N_c + S_w \quad (6)$$

$$S_w = \frac{C_0 S N_0 f_n f_s}{V_w A} \quad (7)$$

where C_0 is effective corrosion rate (g/cm^2.sec), S is area of the system exposed to the coolant for corrosion (cm^2), N_0 is Avogadro's number (6.02x10^{23} atoms/g.mole), A is the atomic weight of target nuclide (g/mole), f_n is natural abundance of target nuclide and f_s is abundance of target nuclide in the system. The rate of change of active nuclides on the surface of the cooling system inside the reactor core is given by;

$$\frac{dn_c}{dt} = \sigma f(t)\phi_0 N_c + \frac{\varepsilon_c Q_c}{V_c} n_w - \left(\frac{k_c}{V_c} + \lambda\right) n_c \tag{8}$$

The following balance gives the rate of change in target nuclei of the core scale;

$$\frac{dN_c}{dt} = \frac{\varepsilon_c Q_c}{V_c} N_w - \left(\frac{k_c}{V_c} + \sigma f(t)\phi_0\right) N_c \tag{9}$$

where V_c is voluthe of deposits within the core (cm^3). The rate of change in active material on the piping surface can be obtained from the following relation;

$$\frac{dn_p}{dt} = \frac{\varepsilon_p Q_p}{V_p} n_w - \left(\frac{k_p}{V_p} + \lambda\right) n_p \tag{10}$$

where V_p is the volume of scale on the piping (cm^3).
The following relation gives target nuclei change rate on the piping scale;

$$\frac{dN_p}{dt} = \frac{\varepsilon_p Q_p}{V_p} N_w - \frac{k_p}{V_p} N_p \tag{11}$$

The above system of coupled differential equations (1-11) is adequate to describe the dynamic response of ACPs under normal operating conditions and a variety of power maneuverings. The system of equations developed in the model is applicable regardless of corrosion pattern. However, we have assumed a uniform corrosion in the coolant circuit and ignored the space distribution effects in our subsequent investigations.

3 The core configuration and flux calculations

The Westinghouse AP-1000 possesses rated core power of 3400 MW_{th}. It contains enriched UO_2 as fuel and light water as a coolant and moderator. The reactor core contains a matrix of fuel rods assembled into mechanically identical 157 fuel assemblies along with control and structural elements. The fuel assemblies are arranged in a pattern, which approximates a right circular cylinder. Three radial regions in the core have different enrichments to establish a favorable power distribution. The enrichment of the fuel in the initial core ranges from 2.35% to 4.50%. The core is designed for a fuel cycle of 18 months with a 93% capacity factor and a region-average discharge burnups of 60,000 MWd/tU. Typical design specifications of the AP-1000 reactor are described in Table 2 [8,9].

The core is surrounded from top, bottom, and in the radial direction by light water and stainless steel reflectors. The thickness of the top, bottom, and radial reflector material is approximately 25 cm, 25 cm and 38 cm[10]. Each of the AP-1000 fuel assemblies consists of a 17×17 square lattice array, out of which 264 are fuel rods, 24 are guide tubes for reactor control and one central instrumentation tube. The Discrete Burnable Absorbers (PYREX) and Integrated Fuel Burnable Absorber (IFBA) rods are used to provide partial control of excess reactivity in the first core. The PYREX rods are removed from the core after the first cycle. The burnable absorber loading controls peaking factors

and prevents the moderator temperature coefficient of the core from becoming positive in normal operating conditions. The PYREX and IFBA rods are arranged in assemblies in three and five different configurations, respectively, giving rise to total nine distinct assembly types in the AP-1000 reactor core. The radial enrichment map of reactor core and configuration of a fuel assembly for AP-1000 is shown in Fig. 2.

Table 2. Typical design specifications of AP-1000 reactor

Parameter	Design value	Parameter	Design value
Power		Mass of UO_2/m (Kg/m)	6.54
Thermal (MW)	3400	Material	UO_2
Electrical (net) (MW)	1090	Pellet diameter (mm)	8.1915
Specific power (kW/kg U)	40.20	Number of fuel rods	41448
Power density ($MW/m^{3)}$	109.70	Rod, OD (mm)	9.50
Core		Diameter gap (mm)	0.1651
Height (m)	4.27	Dimension of FA (mm x mm)	214 x 214
Diameter (m)	3.04	Clad material	ZIRLO
Fuel		Fuel pellet length (mm)	9.83
No. of fuel assemblies	157	Fuel loading, UO_2 (kg)	95974
Rod array dimension	17x17	**Coolant**	
Rods per assembly	264	Pressure (MPa)	15.51
Rod pitch (mm)	12.60	Inlet temperature (°C)	279.44
Clad thickness (mm)	0.5715	Avg. temperature in core (°C)	303.39
Enrichment levels	2.35w/o, 3.40w/o, 4.50w/o	Thermal flow rate of vessel (kg/s)	14300.76

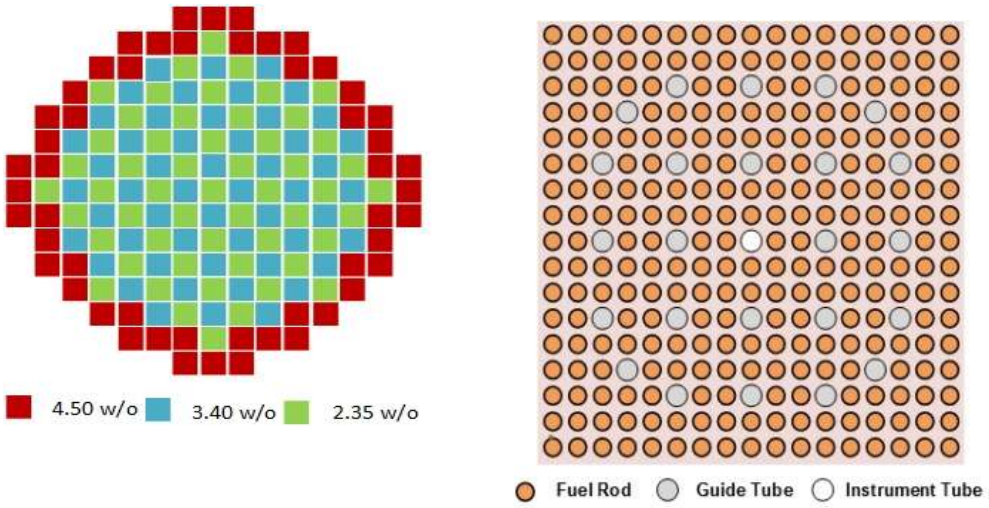

(a) Radial enrichment map **(b) Fuel assembly configuration**

Fig. 2. The radial enrichment map of the reactor core and fuel assembly configuration for AP-1000

3.1 Computing Scheme

Based on the above model, a computer program namely Corrosion Products Activity in AP-1000 (CPA-AP1000), has been developed by executing programming in MATLAB. The overall computational scheme is as shown in Fig. 3. The CPA-AP1000 contains two loops; one loop calculates specific activity under steady-state or power maneuvering conditions, and other moves over different isotopes. After initialization, the program first calculates group fluxes using Tally-4 of the MCNP code. Since the MCNP results are normalized to one source neutron, the result has to be properly scaled in order to get the absolute comparison to the measured quantities of flux. Therefore, the scaling factor is applied in data processing and F4 tally results of core averaged group fluxes are scaled to the desired fission neutron source (power) level using equation 13. The system of coupled differential equations is solved using fourth order Runge-Kutta method.

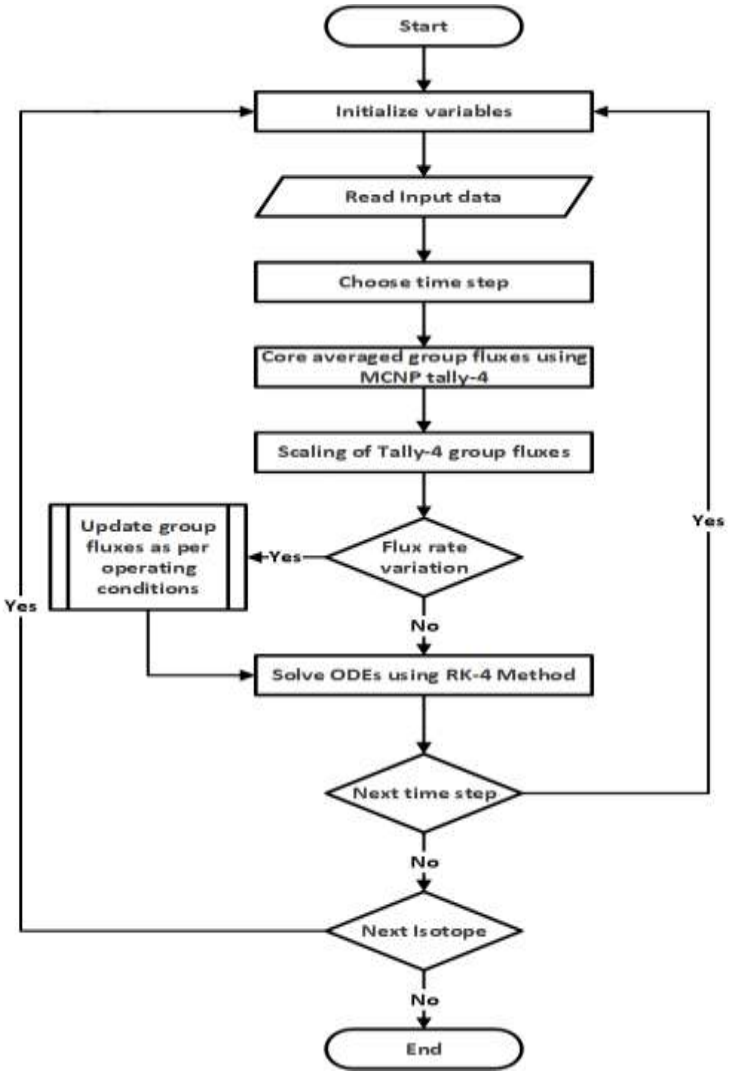

Fig. 3. Flowchart of CPA-AP100 for computing CPA under steady-state operation and flux rate vitiation

4 Results and Discussions

The simulations were started at time t= 0, when reactor was considered to be operating in steady state having no impurities at the initial stage. It has been assumed that the system material corrodes uniformly and homogeneously with constant corrosion rate. The experimental values of different factional exchange rates employed in the present analysis are shown in Table 3 [2,7]. The ion-exchanger removal is the most sensitive parameter to effect CPA values. The detailed effect of ion-exchange removal on saturation specific activity of ^{24}Na was studied using an approach adopted in our previous study [7]. The specific activity of ^{24}Na as a function of reactor operation time was calculated for various values of ion-exchanger removal rate. The aim of the calculation was to demonstrate the well-defined effect of ion-exchanger removal rate on saturation specific by selecting the sufficient data points. The resulting saturation specific activity of ^{24}Na as a function of different ion-exchange removal rate is as shown in Fig. 4.

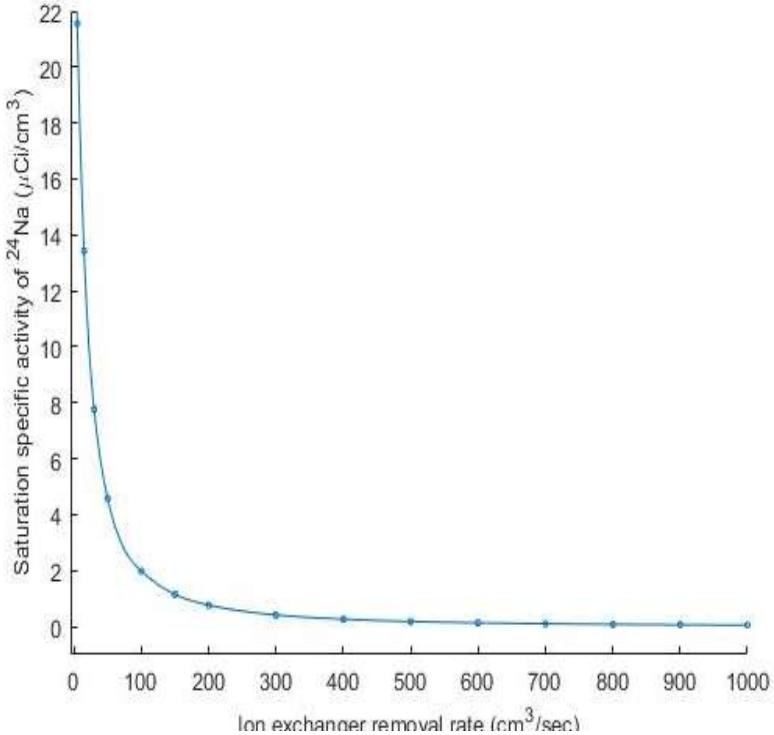

Fig. 4. Saturation specific activity of ^{24}Na as a function of ion-exchange removal rate in primary coolant of AP-1000

The results depicted that the saturation activity is higher enough for low ion-exchanger removal rate and it decreases nonlinearly as ion-exchanger removal rate is increased. When value of $\varepsilon_I Q_I$ approaches 400 cm^3/sec, saturation activity varies with a minor slope and becomes almost constant at 600 cm^3/sec. Therefore, the optimal value of ion-exchange removal rate of 600 cm^3/sec was selected in our subsequent evaluations. The selection of more data points in this study has demonstrated the more clear effect of ion-exchange removal rate on saturation activity, however, trend of the results is the same as obtained in the previous investigation.

Table 3. Fractional exchange rates of a typical PWR

Rate Description	Value1 and Unit	Value2 and Unit
Deposition on core	$\varepsilon_c Q_c/V_w = 5.835x10^{-5}sec^{-1}$	$\varepsilon_c Q_c/V_c = 8.81x10^{-6}sec^{-1}$
Deposition on piping	$\varepsilon_p Q_p/V_w = 1.00x10^{-6}sec^{-1}$	$\varepsilon_p Q_p/V_c = 1.00x10^{-5}sec^{-1}$
Ion-exchanger removal	$\varepsilon_I Q_I/V_w = 5.70x10^{-5}sec^{-1}$	
Resolution ratio for core	$K_c/V_w = 2.918x10^{-6}sec^{-1}$	$K_c/V_c = 4.406x10^{-6}sec^{-1}$
Resolution ratio for piping	$K_p/V_w = 5.0x10^{-7}sec^{-1}$	$K_p/V_p = 5.0x10^{-6}sec^{-1}$
Volume of primary coolant	$V_w = 1.37x10^{7}cm^3$	
Volume of scale on core	$V_c = 9.08x10^{6}cm^3$	
Average corrosion rate	$C_0 = 2.40x10^{-13}\ g/cm^2.sec$	

4.1 Evaluation of ACPs in the primary circuit

The specific activity behavior of ACPs in primary coolant circuit of AP-1000 was studied under full- power neutron flux and design based variation in the flux rate. A typical pattern of neutron flux rate was introduced into the system for this purpose. It was considered that reactor was continuously operated at 100% RTP up to 750 h (i.e. MOC) and then flux rate was slowly reduced. The flux was reduced at a slow rate of 16.67 % of full power flux per hour, which ultimately lead the reactor to operate at 50 % of RTP in almost 3 hours. It was considered that after this variation induced by MSHIM based power transients, reactor operated at 50% of RTP for the rest of the cycle. A typical time-dependent flux pattern depicting such changes in neutron flux with time is shown in Fig. 5.

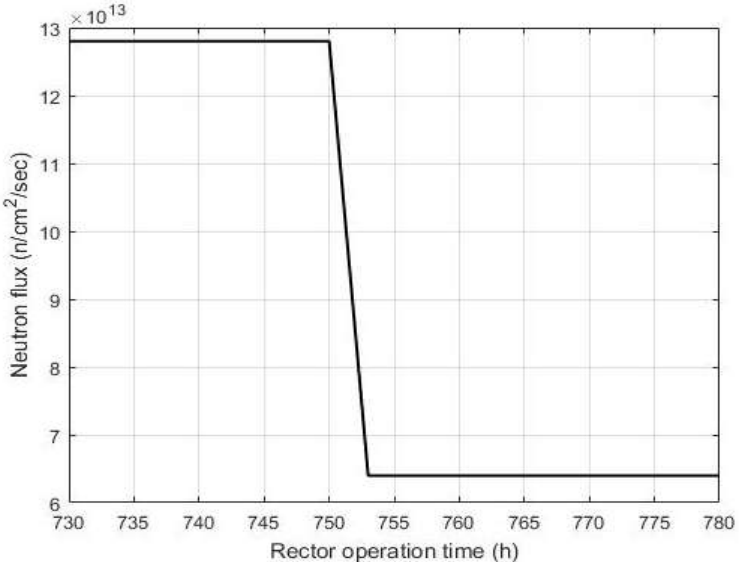

Fig. 5. The variation of neutron flux as a function of reactor operation time

4.1.1 Evaluation of ACPs in the primary coolant

The results for the specific activity buildup behavior of dominant ACPs (^{24}Na, ^{59}Fe, ^{99}Mo, ^{60}Co, ^{56}Mn) in the primary coolant are presented in this section. The simulations for a typical flux rate variation as described in the previous section were run using CPA-AP1000 code. The reactor was operated at 100% RTP without any operational transient up to MOC. After the continuous operation of the reactor at 100% RTP for 750 hours, a slow variation in flux rate variation lead the reactor to 50%

RTP in almost 3 hours. The simulation results showing the behavior of dominant CPs in primary coolant during the complete cycle are presented in Fig. 6. The behavior of various ACPs is described for normal full power operation up to MOC, and for flux rate variation after MOC in following sections.

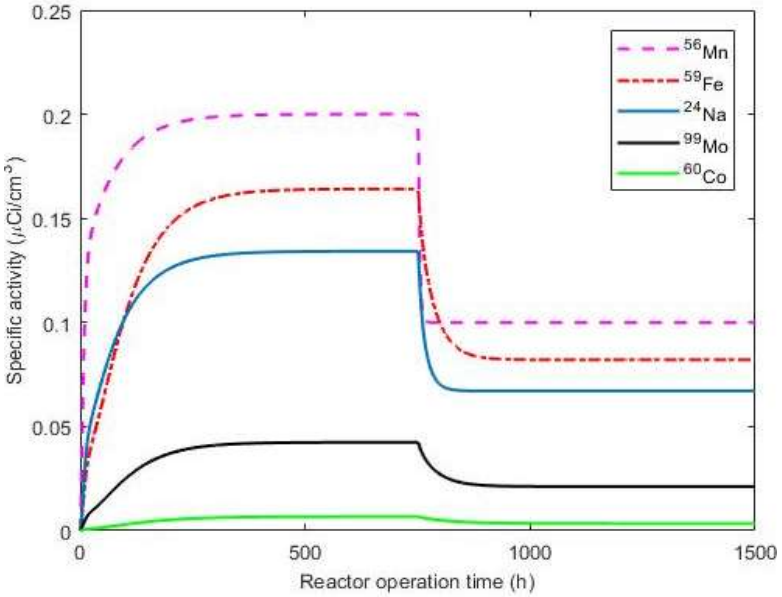

Fig. 6. The Specific activity r of ACPs in primary coolant under normal operation and the design-based variation in neutron flux rate

4.1.1.1 The behavior of ACPs up to Middle of Cycle (MOC)

The response curves of ACPs up to MOC have shown initially rapid increases in activity concentration during normal full power operation, as shown in Fig. 6. The initial rapid increase in specific activity is due to higher corrosion rates during the initial operating period of the reactor. This results in a rapid production of target materials at the beginning and ultimately production of more ACPs. The ACPs start accumulating on the coolant channel piping inner walls surfaces and on the core structures after passing sometime. Furthermore, the ACPs are also removed due to continuous ion-exchange operation and the use of filters. A balance between the removal rate and accumulation of the ACPs on piping and cores surfaces leads to a saturation specific activity value after passing sometime. The ^{56}Mn is the largest contributor to the total specific activity. Its specific activity is about 36.51% of the total specific activity in primary coolant. It has a saturation value of 0.2000 μCi/cm^3. The specific activity response of ^{56}Mn is rapid as compared to all of the other ACPs; it is mainly due to the short half-life as compared to other ACPs of interest. The ^{56}Mn reaches 90% of its saturation value after 100 h of startup time. The ^{59}Fe increases slowly as compared to ^{24}Na. The contribution of ^{59}Fe and ^{24}Na to the total activity is 29.97% and 24.51% respectively. The ^{59}Fe finally approaches a higher saturation value of 0.1641 μCi/cm^3 as compared to the saturation value of 0.1342 μCi/cm^3 for ^{24}Na. The saturation concentrations for ^{59}Fe and ^{24}Na reach 90% of their values in about 200 h and 165 h respectively. The ^{99}Mo and ^{60}Co have longer half-lives as compared to other ACPs under study and they contribute less towards the total specific activity during reactor operation. The contribution

of ^{99}Mo and ^{60}Co to the total specific activity is 7.76% and 1.24% respectively. The saturation activities of ^{99}Mo and ^{60}Co are 0.0425 μCi/cm^3 and 0.0068 μCi/cm^3. The ^{99}Mo and ^{60}Co reach 90% of their values in about 216 h and 280 h respectively. The rounded off values of percentage contribution and saturation level of specific activity for different ACPs in the primary coolant are described in Fig. 7.

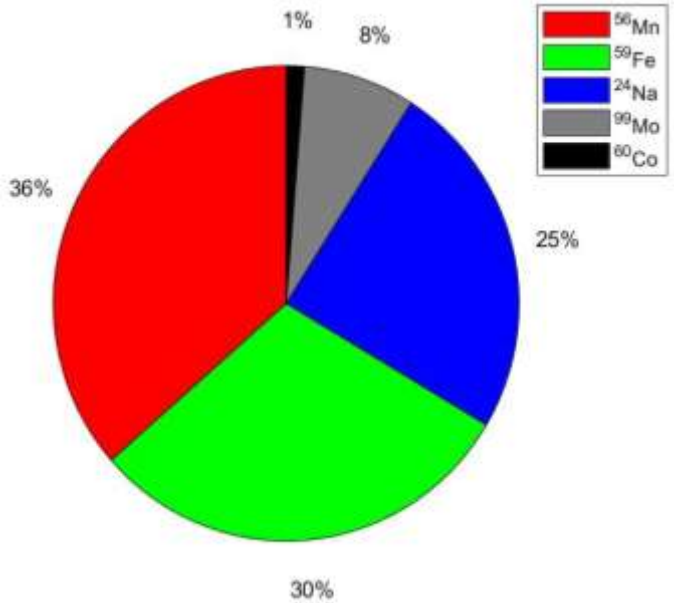

Fig. 7. Percentage contribution of different ACPs in primary coolant under normal full power operation

4.1.2 The behavior of ACPs after the Middle of Cycle (MOC)

The results have demonstrated that during the period of flux variation (750 h–753 h), different ACPs have shown different time-dependent behavior. When flux rate variation was terminated and the reactor was onward operated at 50% RTP, all of ACPs attained a new saturation value. The behavior of specific activity variation after termination of variation in flux is different for different ACPs. The activity due to ^{56}Mn reduced rapidly as compared to all other ACPs. The activity of ^{24}Na reduces at a slower rate as compared to the ^{56}Mn and attains a new saturation value. The ^{59}Fe, ^{99}Mo and Co ^{60} attain a new value after a longer time as compared to ^{56}Mn and ^{24}Na. The detailed behavior of various ACPs during the period of slow variation of neutron flux rate, and settling of saturation specific activity at a reduced value of 50 % RTP is shown in Fig. 8. The short-lived ACPs rapidly attained a new lower saturation value of the specific activity. However, those having longer half-lives sluggishly decayed and their activity retained for a longer period.

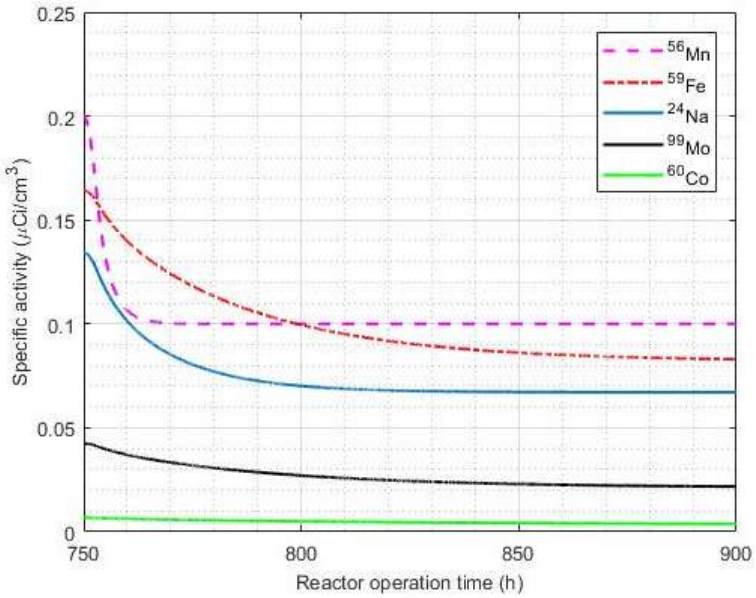

Fig. 8. The specific activity of ACPs during and after the design-based variation in neutron flux rate

4.2 The specific activity of ^{56}Mn in primary coolant and on the inner walls

The time-dependent behavior of specific activity due to ^{56}Mn, on the inner surfaces of primary system walls, is focused in our subsequent investigations. The specific activity behavior of ^{56}Mn in different zones of primary circuit i.e. coolant and inner walls of structure inside and outside reactor core were evaluated. The simulations were run for distinct sessions of plant operation; for normal full power operation up to MOC followed by the design-based variation in the neutron flux rate. The time-dependent variation of specific activity in ^{56}Mn in primary coolant, and on inner walls of both the structures inside the core and piping structure outside the core is shown in Fig. 9. In general, corrosion incidence rate increases steeply at the initial stage of a NPP operation, and over time reaches a saturation state. Therefore, specific activity has depicted initially rapid buildup and finally saturation to a particular value in all zones of the circuit, during normal full power operation. The radioactive materials are accumulated progressively on the system surfaces due to the continuous exchange of ACPs between coolant and system surfaces. During normal operation, specific activity build-up curves in respective zones of the circuit have shown similar behavior. However, the buildup rate and saturation values vary in different zones. The specific activity on the surfaces of the structure inside the core is highest followed by that of coolant. The specific activity on the inner surfaces of the piping structure outside of the core is minimum among all other zones. During the period of (750 h–753 h) design based flux rate variation, the specific activity is also reduced in all zones of the circuit. The specific activity reduction pattern follows a similar trend in all zones. When flux rate variation is terminated, specific activity reaches a new saturation value. The variation of induced by full power operation and neutron flux changes.

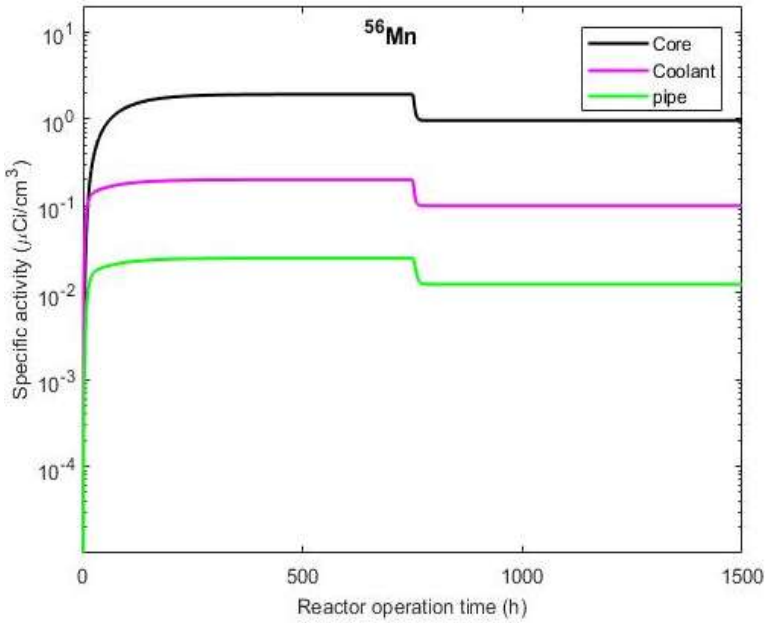

Fig. 9. The specific activity of ^{56}Mn in primary coolant and on inner walls of the primary system during normal operation and design-based variation in neutron flux rate

5 Conclusions

This study has been focused to envisage the specific activity behavior in various zones of the primary circuit of a fresh reactor design. A home developed code CPA-AP1000 is employed to compute the specific activity of ACPs in primary coolant circuit of AP-1000. The activity behavior due to major ACPs is investigated in primary coolant under the steady-state operation and the design-based variation in the neutron flux rate. The results depicted that during normal full power operation, all of ACPs build up at different rates, and finally saturate to constant values. The ACPs have demonstrated time-dependent behaviors during the period of flux variation. When flux rate variation was terminated and the reactor was onward operated at a new power level, all of ACPs attained a new reduced saturation value. The investigations are further extended to compare activity behavior of ^{56}Mn in primary coolant, on inner walls of structural components inside the core, and piping outside the core. The results have shown that specific activity on the surfaces of the structure inside the core is the highest followed by that of coolant. The specific activity on the inner surfaces of the piping structure outside of the core is minimum among all other zones. During the period of design based flux rate variation, the specific activity is also reduced in all zones of the circuit. The specific activity reduction pattern follows a similar trend in all parts of the circuit. When flux rate variation is terminated, specific activity in all parts of the circuit also attains a new saturation value. The estimation of activity behavior of ACPs under normal operation and design-based variation of flux rate is helpful in envisaging the corresponding radiation levels. The detailed behavior of other major ACPs in different parts of the primary circuit needs further investigations.

6 References

[1] Rafique M, Mirza N, Mirza S, et al. Review of computer codes for modeling corrosion product transport and activity build-up in light water reactors. NUKLEONIKA, 2010, 55: 263-269.

[2] Mirza A, Mirza N, Mir I. Simulation of corrosion product activity in pressurized water reactors under flow rate transients. Annals of Nuclear Energy, 1998, 25 (6): 331-345.

[3] Génin JB, Brissonneau L, Gilardi T. OSCAR-Na: A New Code for Simulating Corrosion Product Contamination in SFR. 2016, 3. **DOI:** 10.1007/s40553-016-0094-9

[4] Song JS, Cho HJ, Jung MY, et al. A Study on the Application of CRUDTRAN Code in Primary Systems of Domestic Pressurized Heavy-Water Reactors for Prediction of Radiation Source Term. Nuclear Engineering and Technology, 2017, 49 (3): 638-644. **DOI:** 10.1016/j.net.2016.11.005

[5] Li L, Zhang J, He S, et al. The development of two-phase three-node model used to simulate the transport of ACPs. 2017, 97: 99-105. **DOI:** 10.1016/j.pnucene.2016.12.015

[6] Shuran M, Jia J, Yichen B, et al. Modelling of materials corrosion inside RCS based on mixed-conduction model. Proceedings of 8th International Symposium on Symbiotic Nuclear Power Systems for 21st Century Chengdu, China, September 26-28, 2016.

[7] Mahmood F, Hu H, Cao L. Dynamic response analysis of corrosion products activity under steady state operation and Mechanical Shim based power-maneuvering transients in AP-1000. Annals of Nuclear Energy, 2018, 115: 16-26. **DOI:** 10.1016/j.anucene.2018.01.009

[8] Westinghouse. AP1000 Design Control Document, Rev. 19, 2011. https://www.nrc.gov/docs/ML1117/ML11171A500.html

[9] Stefani GL, Rossi PR, Maiorino JR, et al. Neutronic and thermal-hydraulic calculations for the AP-1000 NPP with the MCNP6 and Serpent codes. 2015 International Nuclear Atlantic Conference - INAC 2015, São Paulo, Brazil, October 4 - 9, 2015.

[10] Elsawi MA, Hraiz ASB. Benchmarking of the WIMS9/PARCS/TRACE code system for neutronic calculations of the Westinghouse AP1000™ reactor. Nuclear Engineering and Design, 2015, 293: 249-257. **DOI:** 10.1016/j.nucengdes.2015.08.008